

A TES X-ray Spectrometer for NSENSE

Christine G. Pappas, Malcolm Durkin, Joseph W. Fowler, Kelsey M. Morgan, Joel N. Ullom
National Institute of Standards and Technology
325 Broadway
Boulder, CO 80305, USA
Email: Christine.Pappas@NIST.gov

Department of Physics
390 UCB
University of Colorado Boulder,
CO 80309-0390

W. Bertrand Doriese, Gene C. Hilton, Galen C. O’Neil, Daniel R. Schmidt, Paul Szypryt, Daniel S. Swetz
National Institute of Standards and Technology
325 Broadway
Boulder, CO 80305

Abstract—The Non-destructive Statistical Estimation of Nanoscale Structures and Electronics (NSENSE) instrument for IARPA’s Rapid Analysis of Various Emerging Nanoelectronics (RAVEN) program is a tabletop X-ray tomography prototype designed for three-dimensional imaging of integrated circuits with 10 nm spatial resolution. Here, we describe the X-ray detector for NSENSE, our 240-pixel superconducting Transition-edge Sensor (TES) spectrometer. It achieves an energy resolution of 12 eV at 8.0 keV at a photon rate of 200 counts per second per pixel. Precise energy resolution is necessary for the NSENSE concept, and is not achievable with any other energy dispersive detector. We plan to build TES spectrometers of 3,000 and 10,000 pixels for RAVEN Phase II and III, respectively, for faster imaging.

Keywords—TES, X-ray, tomography

I. INTRODUCTION

The Non-destructive Statistical Estimation of Nanoscale Structures and Electronics (NSENSE) X-ray tomography instrument for IARPA’s Rapid Analysis of Various Emerging Nanoelectronics (RAVEN) program aims to produce three-dimensional images of integrated circuits (ICs) with 10 nm spatial resolution [1]. While three-dimensional imaging with spatial resolution on this scale has been demonstrated by X-ray tomography and ptychography experiments using the high photon flux, collimated, phase-coherent X-ray beam that can only be produced at synchrotron or linear accelerator facilities, NSENSE would be the first tabletop apparatus with this capability [2]. The NSENSE X-ray source is produced by a scanning electron microscope (SEM) e-beam incident on a gold film, which generates X-rays at the gold emission L-lines. To achieve 10 nm spatial resolution with this source, NSENSE will use Transition-edge Sensor (TES) X-ray microcalorimeters as the detectors for the experiment.

TES X-ray microcalorimeters can measure the energy of individual X-ray photons with a precision better than one part in 1000, exceeding any other energy-dispersive detector. They can be engineered to maintain their precise energy resolution

over a broad energy range. These detectors are naturally arranged into pixelated arrays, yielding a large collection solid angle which provides geometric diversity for tomography with the NSENSE isotropic X-ray source. They also have a high quantum efficiency and provide a high SNR since the narrow spectral response integrates less background (or noise), making them ideal for photon-starved experiments like NSENSE.

The energy resolving power of the TES provides several further advantages for the NSENSE experiment. First, with the TES, we can discriminate between photons created in the gold film, at the characteristic gold emission L-lines, and X-rays created by Bremsstrahlung or fluorescence in other metals by scattered electrons or X-rays. This effectively creates an isotropic X-ray source with a source distribution known to be confined to the gold target material. Due to electron scattering this source region is not conformal to the incident probe beam, and instead electrons scatter and diffuse, which broadens the source region. However, it is possible to maintain high spatial resolution by using a sufficiently thin target material and modeling the expected source distribution with Monte Carlo tools during inversion processing.

Second, we can use an X-ray source with multiple emission lines, as the TES can discern between them. This is especially useful when K-edge tomography (or more generally, spectral computed tomography) is possible [3]. In Phase-I of NSENSE, we will use the six most prominent gold emission L-lines, ranging in energy from about 8.5-13.4 keV. In Phases II and III of NSENSE, we plan to use nano-patterned targets of multiple metals with differing emission lines. This will allow us to increase the flux of the SEM beam and hence the spot size without losing spatial resolution.

Third, when the TES is used beam-side (instead of in transmission-style measurement) it augments the lower spectral resolution energy-dispersive X-ray spectroscopy (EDX) sensor, and may be used for X-ray fluorescence mapping of the device layer of an appropriately prepared IC sample. Here, the enhanced SNR of the TES is significant as otherwise the characteristic lines from the trace elements in the device

DISTRIBUTION STATEMENT A. Approved for public release: distribution is unlimited.

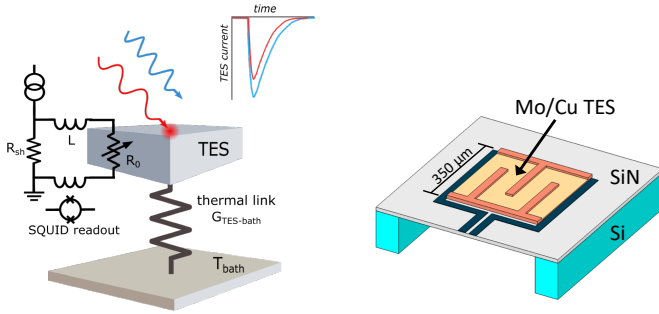


Fig. 1. *Left:* Schematic of a voltage-biased TES microcalorimeter. When the TES island absorbs a photon, there is a downward pulse in the TES current, which is read out by a SQUID multiplexing system. *Right:* Diagram of how the TES microcalorimeter is implemented in practice. The $350\ \mu\text{m} \times 350\ \mu\text{m}$ Mo/Cu TES with Mo leads is suspended on a SiN_x membrane, which provides a weak link to the silicon substrate thermal bath. The interdigitated Cu bars running across the TES are noise-mitigating features. A bismuth absorber, not pictured here, is deposited on top of the TES to increase the quantum efficiency.

layer would never rise above the Bremsstrahlung background. With the TES spectral resolution it is also possible to resolve emission lines from multiple elements that would overlap if a detector with less precise energy resolution were used.

Here, we describe the NSENSE TES spectrometer that will be used in Phase I of RAVEN. During the 40 day Phase I period, we aim to make a three-dimensional, 10 nm spatial resolution image of a small area of a 14 nm technology node integrated circuit. In subsequent phases, we plan to increase the imaging speed of the instrument by using larger, faster TES arrays.

II. SPECTROMETER DESIGN

A TES microcalorimeter measures the energy of individual photons via a thermal process similar to a classic macroscopic calorimeter. An incoming photon is absorbed by an "island" that is weakly thermally connected to a surrounding thermal bath, as shown in Fig. 1. The island temperature quickly increases after the photon is absorbed then decays back to the ambient value. This pulse in temperature is sensed by a TES on the island. A TES is a superconducting thin film voltage-biased into the transition region between the superconducting and normal states, where it acts as a very sensitive resistive thermometer. When a photon is absorbed, the signal we measure is a transient reduction in the current through the TES [4]. The photon energy is calculated through the statistically optimal determination of the pulse size [5].

The NSENSE TES spectrometer has 240 TES microcalorimeter pixels, cooled to about 100 mK with an adiabatic demagnetization refrigerator (ADR) to reduce thermal noise. The TES signals must be multiplexed before being routed to room temperature, to reduce thermal loading on the refrigeration system. TES arrays have been successfully multiplexed with a variety of approaches, all of which use SQUIDs as low-noise current amplifiers with fast response

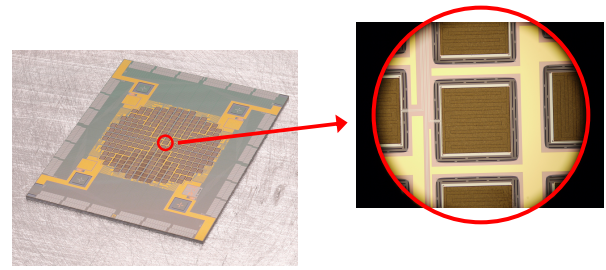


Fig. 2. *Left:* A 240 pixel TES microcalorimeter array like the one used for NSENSE. The chip size is $19\ \text{mm} \times 15\ \text{mm}$. *Right:* A magnified view of the TES detectors. The TES is the $350\ \mu\text{m} \times 350\ \mu\text{m}$ brown square. Behind the TES and extending to the grey region around it, the silicon has been removed by a DRIE backside etch so that the TES is suspended by a SiN_x membrane. The dashed lines in the grey region are the perforations in the membrane discussed in the text. In the yellow areas surrounding the TESs, a gold heat sinking layer has been deposited on top of the SiN_x .

times [6]. Here, we use the most mature of the available multiplexing schemes, time-division multiplexing (TDM) [7].

This TES spectrometer model has been used for a variety of applications, and was optimized differently for each one [8]. For NSENSE, we want the spectrometer to measure photons in the energy range of the most prominent Au emission L-lines, about 8-14 keV, with the energy resolution necessary for NSENSE to achieve 10 nm spatial resolution. To maximize imaging speed, the spectrometer should count as many of the photons incident on the array as possible. The photon flux on the array will be limited by the capabilities of the source. Based on end-to-end simulations, the spectrometer requirements are a dynamic range of at least 14 keV, a count rate capability of 100-300 counts per second (cps) per pixel, and an energy resolution of 20 eV or better at 200 cps and 8 keV.

Historically, TES spectrometers have been operated in low flux environments, at count rates less than 10 cps per pixel, with a premium placed on achieving high resolving power. The NSENSE performance metrics are therefore in a new parameter space for this technology. To achieve these specifications, we started with a trusted TES spectrometer design for high resolution detection of 6 keV photons at low count rates. We then increased the dynamic range and count rate capabilities of the instrument at some expense to the energy resolution.

The two main challenges when operating a TES spectrometer at high count rates are "pileup" and crosstalk between readout channels. The pileup effect refers to the case when a photon arrives before the detector has completely recovered after a previous event and the pulses overlap. Because TES detectors are non-linear, it is difficult to determine the energy of either photon in this case. While pileup can be partially mitigated with advanced analysis techniques, it is necessary to decrease the detector response time in hardware in order to make large increases in the spectrometer count rate capability [11] [12].

Each NSENSE TES is a $350\ \mu\text{m} \times 350\ \mu\text{m}$ square molybdenum/copper (Mo/Cu) bilayer with 8 noise-mitigating copper

interdigitated bars [8]. The T_c of the TES bilayer can be adjusted by changing the thicknesses of the superconducting molybdenum layer and the normal metal copper layer, which suppresses the intrinsic T_c (~ 915 mK) of the bare molybdenum film via the proximity effect [9]. The TES is suspended on a silicon nitride (SiN_x) membrane to provide a weak thermal link to the surrounding silicon substrate, as shown in the schematic in Fig. 1 and the photo of our real devices in Fig. 2. Perforations in the SiN_x membrane are used to decrease the thermal conductance as necessary, as shown in Fig. 2 [10]. A bismuth layer on top of the TES aids in the absorption of X-rays and adds negligible heat capacity. For NSENSE, the bismuth layer is 4.4 ± 0.2 μm thick, yielding a calculated quantum efficiency of 44% at 10 keV.

The TES microcalorimeter is usually designed to have a dynamic range near its application's maximum photon energy, as increasing the dynamic range degrades energy resolution [4]. The dynamic range is roughly proportional to the TES heat capacity. For NSENSE, we increased the TES T_c from 100 mK to 130 mK by adjusting the Mo and Cu layers of the TES bilayer to 60 ± 2 nm and 220 ± 6 nm thick, respectively. As the TES heat capacity scales linearly with temperature, this increased the heat capacity, and thereby the dynamic range, by a factor of about 30%. The higher T_c of the TES also lets us operate our ADR at a base temperature of 100 mK, instead of the usual 60-80 mK, which increases the hold time of the ADR between thermal cycles.

To minimize pileup at the NSENSE count rate of 100-300 cps per pixel, we decreased the detector response time of the original spectrometer design. The detector speed is limited by the maximum slew rate (time derivative of the pulse signal) that can be tracked by the multiplexing readout. For NSENSE, we increased the maximum TES signal slew rate of our standard TDM design, when operated on the lower noise steep slope part of the first stage SQUID (SQ1) curve, to about 0.9 A/sec. This was done by decreasing the coupling between the TES and the SQ1 by a factor of about 8/3.

The response time of a TES microcalorimeter to a photon is proportional to C/G , where C is the heat capacity of the island and G is the thermal conductance between the island and the thermal bath. The actual response time is shorter than C/G due to negative electrothermal feedback and depends on several additional device parameters, such as the dimensionless logarithmic derivative of the TES resistance with respect to temperature (α) and current (β) [4]. The most straightforward way for us to increase the detector speed is to increase G . For NSENSE, we increased G by adjusting the perforation pattern in the SiN_x membrane. The G value was selected based on TES simulations such that the response time would be as short as possible while staying safely within the slew rate constraints of the readout.

III. SPECTROMETER CHARACTERIZATION AND PERFORMANCE

Here, we discuss the measured properties and performance of the NSENSE spectrometer. The detectors are operated at

T_c	130 mK
R_n	12 m Ω
R_{sh}	350-700 $\mu\Omega$
L	300 nH
Bias point	30% R_n
T_b	100 mK
G	600 pW/K
C	1.2 pJ/K
α	95
β	0.8

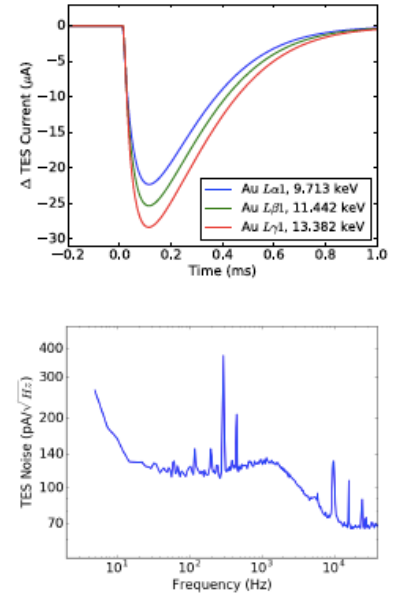


Fig. 3. *Left:* Table of detector properties. The G , C , α , and β values given are for the operating bias point of 30% R_n and bath temperature of 100 mK. *Upper Right:* Pulses from a typical detector at Au L-lines. *Lower Right:* Noise spectrum of a typical detector at its operating point on a log-log plot. Here, we are multiplexing 28 rows and dwelling 240 ns per row.

a bath temperature of 100 mK and biased to about 30% of their normal resistance. The TES is effectively voltage-biased by applying a bias current to the TES in parallel with a small shunt resistor, R_{sh} , as shown in Fig. 1. The total inductance in the bias circuit, L , was selected such that the detector is nearly critically damped [4]. The properties of a typical detector at this operating point are shown in Fig. 3. The thermal conductance between the island and the bath was calculated by the standard method from IV curves taken at a range of bath temperatures. Then, C , α , and β were determined with complex impedance measurements [13].

The pulse signals produced by a typical detector in this array in response to photons in the energy range of the most prominent Au L-lines are shown in Fig. 3. The dead time of these detectors, which we define here as the time from the beginning of the pulse to the time when the pulse is at 10% of its peak value, is about 700-800 microseconds, depending on the detector and photon energy. This is about three times faster than pulses from the original detector design. The maximum slew rate of the pulses at 13.5 keV is about 0.8 A/sec, within the range of the optimized NSENSE TDM readout.

The noise spectrum of a typical TES at its operating point is also shown in Fig. 3. The TES noise is low pass filtered by the L/R rolloff of the bias circuit. At high frequencies, above about 10 kHz here, all the noise can be attributed to the readout. The readout noise level here is 70 pA/ $\sqrt{\text{Hz}}$, about 8/3 higher than the original TDM design due to the reduced coupling between the TES and the SQ1. At high count rates, we are dominated by crosstalk effects, and this extra readout noise does not significantly affect the overall energy resolution.

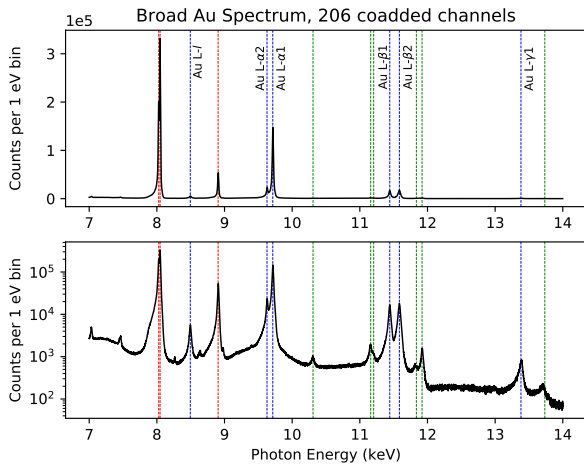


Fig. 4. Linear (*Top*) and logarithmic (*Bottom*) plots of the emission spectrum from a mixed gold and copper target measured by the NSENSE array. A photon flux of 200 cps was incident on each pixel. The energy spectra of the 206 good detectors in the array were summed to create this plot. The blue, labeled lines are the six brightest Au emission L-lines, which will be used for imaging in NSENSE. The green lines are lower probability Au emission events. The red lines are at the Cu $K\alpha 1$, $K\alpha 2$, and $K\beta 1$ emission line energies.

The detectors in this array can measure photons of energy above 14 keV, meeting the dynamic range requirements of the experiment. The measured energy spectrum of emission from a mixed copper and gold target fluoresced with an X-ray tube source is shown in Fig. 4. The Cu K-lines and the most prominent Au L-lines are clearly resolved from the background. The spectrum shown here is the sum of the spectra from the 206 functional detectors in the array. It should be noted that for NSENSE, each TES pixel will be analyzed separately for tomography.

While the design changes necessary to yield faster detectors with higher dynamic range do degrade the energy resolution slightly, we are still within NSENSE targets. The intrinsic energy resolution of these detectors, which we define as the energy resolution of an individual (not multiplexed) detector operated at low count rates of 1-2 cps, is about 6 eV at 8.0 keV. When multiplexing is used to read out all the detectors in the array at once, the energy resolution degrades slightly. As the photon rate is increased, the energy resolution starts to degrade more due to an increase in crosstalk events. By crosstalk, we mean that when a photon pulse occurs in some detector, a signal about 1000 times smaller than the original will be seen in some other readout channels. The crosstalk mechanism is electrical, and we do not observe thermal crosstalk in these detectors [8].

Crosstalk mitigation was particularly important due to NSENSE's high count rate requirement. To reduce crosstalk, we made changes to cryostat wiring, SQUID operation, TDM timing parameters, and pulse record length. Cryostat wiring was extensively redesigned to reduce electrical crosstalk, with the addition of a ground plane to reduce capacitive coupling between wires. The series array SQUID amplifier was made

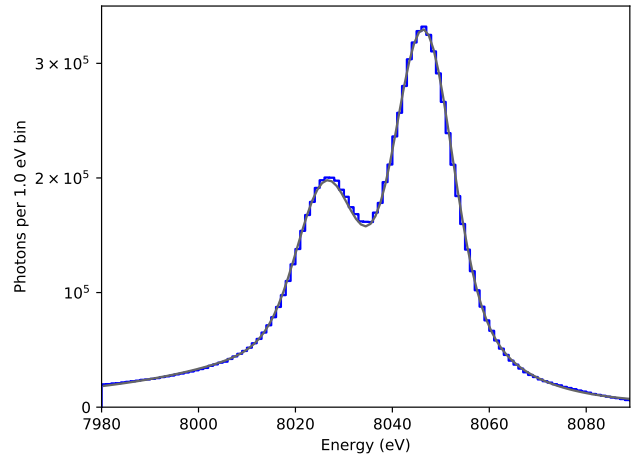


Fig. 5. The spectrum of copper $K\alpha$ emission, containing over 10^7 X-ray photons from 206 TESs combined. The overlaid fit (in gray) assumes the intrinsic line shape given in Hölzer et al (1997) convolved with our energy-response function [14]. The energy-response has a Gaussian component of FWHM 12.04 ± 0.02 eV (statistical uncertainty only), convolved with a combination of a delta function and exponential tails to both low and high energy.

less susceptible to electrical crosstalk by operating on the SQUID shallow slope. TDM timing parameters were set to minimize crosstalk between channels. We used a settling time of 160 ns and a sampling time of 80 ns, for a total row dwell time of 240 ns. Lastly, the record length used in pulse analysis was shortened to 0.54 ms total, 30% of which was pre-trigger. While shortening the record length results in an energy resolution penalty at low rates, there is a lower probability for crosstalk events in the shorter record, leading to better overall energy resolution at high count rates.

An energy spectrum of Cu $K\alpha$ emission produced by this array operating at 200 cps per pixel is shown in Fig. 5. The spectrum is given by the actual Cu $K\alpha$ emission line shape, convolved with the detector array's energy-response function. The ideal energy-response function is a Gaussian, and its full-width at half maximum gives the energy resolution of the detector. Non-ideal behavior of the X-ray absorbing layers can produce long time-scale thermal effects that smear the energy response to lower energies [15]. In such sensors, the energy response is well described by a Gaussian plus the convolution of that Gaussian with a one-sided, low-energy exponential.

When the NSENSE spectrometer is operated at high photon rates, we observe both a low-energy and high-energy exponential tail in the energy-response function. While some of the low-energy tail is also observed at low count rates and can be attributed to absorber effects, we believe that the high-energy tail and a portion of the low-energy tail are produced by crosstalk events. At 200 cps, 20% of the photon events are in the high-energy tail portion of the energy response function, 27% are in the low-energy tail, and 53% are in the pure Gaussian. The pure Gaussian has a full-width at half-maximum (FWHM) of 12.04 ± 0.02 eV. The high-energy tail

energy-response function is this Gaussian convolved with a positive exponential distribution with a mean of 12 eV, while the low-energy tail is described by the Gaussian convolved with a negative exponential distribution with a mean of 33 eV.

In Fig. 6, the effect of count rate on the energy resolution, as defined by the metric discussed above, is shown. An energy resolution of 15 eV or better is maintained up to 300 cps. It should be noted that due to the large percentage of photon events in the tails, the energy resolution given by the Gaussian is not an entirely meaningful number here. In the future, we plan to develop an energy resolution metric that also encapsulated the crosstalk effects in the tails.

The spectra shown here were generated by traditional optimal filtering analysis, so pulses containing any pileup were rejected [5]. We can reject fewer pulses and maintain good energy resolution using advanced pileup analysis techniques. In general, there is a tradeoff between throughput and energy resolution. New pileup analysis techniques are currently in development that build on previously published results [12]. With these techniques, we estimate that we can maintain the energy resolution cited here while achieving 80-90% throughput.

CONCLUSIONS AND FUTURE WORK

We have built a 240-pixel TES spectrometer optimized for NSENSE that achieves an energy resolution of 12 eV at 8.0 keV at a photon rate of 200 cps per pixel. We will use this spectrometer during Phase I of RAVEN, then upgrade to larger, faster TES arrays in Phase II and Phase III for faster imaging. Using microwave SQUID multiplexing readout (μ mux), we will produce arrays of 3,000 pixels for Phase II and 10,000 pixels for Phase III [16] [17].

The μ mux readout has a bandwidth of 4 GHz per multiplexing group, a factor of about 40 increase over TDM. This higher bandwidth enables a higher total photon count rate per multiplexing group. One can use this higher bandwidth to read out more detectors per multiplexing group and/or increase the count rate capabilities of individual detectors. In addition to increasing the pixel count of the arrays, using μ mux for Phase II and III of RAVEN will allow us to increase the speed of each detector as necessary, depending on how much flux the source can produce.

To support the larger arrays and their readout cables, we will upgrade to a dilution refrigerator with higher cooling power than the ADR used for Phase I [18]. The dilution refrigerator base temperature will also be lower than the ADR described here, which will further lower the TES noise. While the technology needed for the Phase II and Phase III arrays is already existing and proven, we also have a more theoretical path towards arrays of 100,000 pixels within the next 10 years.

ACKNOWLEDGMENT

The NSENSE concept was developed by Eugene Lavelly and his research group at BAE Systems Inc. We would like to acknowledge support from IARPA grant 16002D2017-1706230005. Paul Szypryt is supported by a National Research Council Post-Doctoral Fellowship.

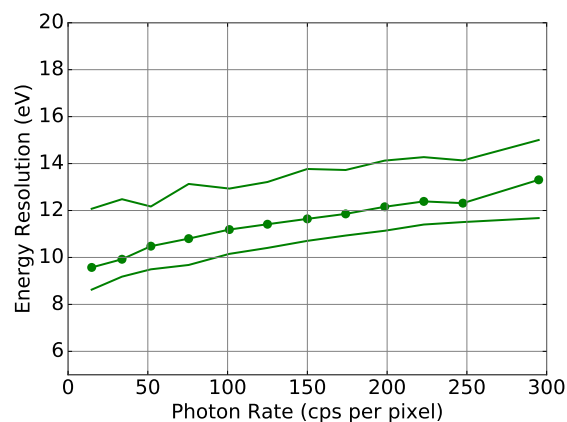


Fig. 6. Energy resolution of the Copper $K\alpha$ emission spectrum as a function of photon rate, the number of photons per second incident on each pixel. Here, the energy resolution is calculated by the same procedure as in Fig. 5. The data points are the median over the detectors in the array, while the lines above and below are the 75th and 25th percentile, respectively.

REFERENCES

- [1] E. M. Lavelly, P. R. Moffitt, and C. L. Willis, "Integrated X-ray Transmission Tomography and Scanning Electron Microscope," This Proceedings.
- [2] F. Pfeiffer, "X-ray ptychography," *Nature Photonics*, vol. 12, no. 1, pp. 9-17, Dec. 2017.
- [3] J. P. Schlomka et al., "Experimental feasibility of multi-energy photon-counting K-edge imaging in pre-clinical computed tomography," *Physics in Medicine and Biology*, vol. 53, no. 15, pp. 4031-4047, Jul. 2008.
- [4] K. Irwin and G. Hilton, "Transition-Edge Sensors." In: Enss C. (eds) *Cryogenic Particle Detection. Topics in Applied Physics*, vol. 99. Springer, Berlin, Heidelberg
- [5] J. W. Fowler et al., "The Practice of Pulse Processing," *Journal of Low Temperature Physics*, vol. 184, no. 1-2, pp. 374-381, Dec. 2015.
- [6] J. N. Ullom and D. A. Bennett, "Review of superconducting transition-edge sensors for X-ray and gamma-ray spectroscopy," *Superconductor Science and Technology*, vol. 28, no. 8, p. 84003, Jul. 2015.
- [7] W. B. Doriese et al., "Developments in Time-Division Multiplexing of X-ray Transition-Edge Sensors," *Journal of Low Temperature Physics*, vol. 184, no. 1-2, pp. 389-395, Dec. 2015.
- [8] W. B. Doriese et al., "A practical superconducting-microcalorimeter X-ray spectrometer for beamline and laboratory science," *Review of Scientific Instruments*, vol. 88, no. 5, p. 53108, May 2017.
- [9] J. M. Martinis, G. C. Hilton, K. D. Irwin, and D. A. Wollman, "Calculation of T_c in a normal-superconductor bilayer using the microscopic-based Usadel theory," *Nuclear Instruments and Methods in Physics Research Section A: Accelerators, Spectrometers, Detectors and Associated Equipment*, vol. 444, no. 1-2, pp. 23-27, Apr. 2000.
- [10] J. P. Hays-Wehle, D. R. Schmidt, J. N. Ullom, and D. S. Swetz, "Thermal Conductance Engineering for High-Speed TES Microcalorimeters," *Journal of Low Temperature Physics*, vol. 184, no. 1-2, pp. 492-497, Jan. 2016.
- [11] B. K. Alpert et al., "Note: Operation of gamma-ray microcalorimeters at elevated count rates using filters with constraints," *Review of Scientific Instruments*, vol. 84, no. 5, p. 56107, May 2013.
- [12] J. W. Fowler et al., "Microcalorimeter Astrophysics at high pulse rates: A multi-pulse fitting technique," *The Astrophysical Journal Supplement Series*, vol. 219, no. 2, p. 35, Aug. 2015.
- [13] M. A. Lindeman et al., "Impedance measurements and modeling of a transition-edge-sensor calorimeter," *Review of Scientific Instruments*, vol. 75, no. 5, pp. 1283-1289, May 2004.
- [14] G. Hölzer, M. Fritsch, M. Deutsch, J. Härtwig, and E. Förster, " $K\alpha_{1,2}$ and $K\beta_{1,3}$ x-ray emission lines of the 3d transition metals," *Physical Review A*, vol. 56, no. 6, pp. 4554-4568, Dec. 1997.
- [15] D. Yan et al., "Eliminating the non-Gaussian spectral response of X-ray absorbers for transition-edge sensors," *Applied Physics Letters*, vol. 111, no. 19, p. 192602, Nov. 2017.

- [16] J. A. B. Mates et al., "Simultaneous readout of 128 X-ray and gamma-ray transition-edge microcalorimeters using microwave SQUID multiplexing," *Applied Physics Letters*, vol. 111, no. 6, p. 62601, Aug. 2017.
- [17] D. Li et al., "TES X-ray Spectrometer at SLAC LCLS-II," *Journal of Low Temperature Physics*, vol. 193, no. 5-6, pp. 1287-1297, Sep. 2018.
- [18] K. M. Morgan et al., "Use of Transition Models to Design High Performance TESs for the LCLS-II Soft X-ray Spectrometer," *IEEE Transactions on Applied Superconductivity* *Under Review*